Material model for wood

C. Sandhaas

Institute for Timber Structures and Building Construction, Karlsruhe Institute of
Technology, Germany
Delft University of Technology, the Netherlands

J.W.G. van de Kuilen

Delft University of Technology, the Netherlands
Holzforschung München, University of Technology Munich, Germany

**Wood is highly anisotropic and shows ductile behaviour in compression and brittle
behaviour in tension and shear where both failure modes can occur simultaneously. A 3D
material model for wood based on the concepts of continuum damage mechanics was
developed. A material subroutine containing the developed model was implemented into a
standard FE framework. Eight stress-based failure criteria were derived in order to formulate
piecewise defined failure surfaces. The damage development of wood was controlled by nine
damage variables. Embedment tests using three different wood species (spruce, beech, azobé)
were carried out whose results were compared to modelling outcomes. The failure modes
could be identified and the general shape of the load-displacement curves agreed with the
experimental outcomes up to a numerical limit.**

*Key words: Constitutive model, timber, wood, continuum damage mechanics, finite element
method*

1 Introduction

Wood and timber joints are difficult to model. Apart from their heterogeneity, material-
specific issues lead to numerical problems: strong anisotropy with different strengths in
tension and compression and ductile and brittle failure modes occurring simultaneously.
Existing approaches are mostly based on specific approaches for different problem classes.
Brittle problems can be modelled with fracture mechanics approaches within a continuum
framework (*e.g.* Schmid [2002], Ballerini and Rizzi [2005]) or discrete lattice models (*e.g.*
Wittel et al. [2005], Reichert [2009], Nagy [2010]). For ductile problems, classical flow
theory of plasticity in combination with the Hill criterion (e.g. Dias et al. [2010]), the

Hoffman criterion (e.g. Xu et al. [2009]) or even the Tsaï-Wu criterion (e.g. Bouchaïr et al. [1995], Dorn [2012]) is generally used. To overcome the need of separate approaches for different problem classes, multi-surface plasticity models have been developed (Fleischmann [2005], Grosse [2005], Schmidt and Kaliske [2006]). Recent approaches use multiscale modelling techniques where representative volume elements are derived starting at chemical level and scaling up the hierarchical levels of wood [Hofstetter et al., 2005]. Also hybrid approaches assigning different constitutive laws to describe the mechanical behaviour of wood in parallel resp. perpendicular direction (e.g. Bocquet [1997], Toussaint [2010]. Toussaint uses crushable foam laws to model behaviour perpendicular-to-grain) or models combining cohesive zone interface elements that represent splitting failures in combination with flow theory of plasticity for compression failures exist (e.g. Franke [2008]).

However, multi-surface plasticity models and multiscale models are not readily available for timber engineers nor are they easy to handle as often, no clearly defined material properties are implemented. Furthermore, multiscale models are limited to elastic problems at the current state-of-the-art and are hence not suitable. The last mentioned hybrid approaches represent practical solution strategies, but for instance, models using cohesive zone interfaces need pre-defined splitting planes and are no integral approaches to model the 3D mechanical behaviour of wood.

Therefore, in this paper, a general approach combining the above mentioned issues in one single 3D material model was developed, within the framework of continuum damage mechanics (CDM). The developed constitutive model was used to predict the results of embedment tests which are important tests to assess the load carrying capacity and mechanical behaviour of timber joints.

2   Definitions

Material directions and arrays must be defined before introducing the material model. Both are given in Equation (1) and Figure 1. The common indices in timber engineering are used, e.g. index 90 = direction perpendicular-to-grain, index v = longitudinal shear, index $roll$ = rolling shear (σ_{23}), index L = longitudinal direction (Figure 1).

$$\begin{aligned}
\boldsymbol{\sigma} &= \begin{bmatrix} \sigma_L & \sigma_R & \sigma_T & \sigma_{LR} & \sigma_{LT} & \sigma_{RT} \end{bmatrix}^T = \begin{bmatrix} \sigma_0 & \sigma_{90R} & \sigma_{90T} & \sigma_{vR} & \sigma_{vT} & \sigma_{roll} \end{bmatrix}^T \\
&= \begin{bmatrix} \sigma_{11} & \sigma_{22} & \sigma_{33} & \sigma_{12} & \sigma_{13} & \sigma_{23} \end{bmatrix}^T
\end{aligned}$$

(1)

As already stated, wood is an anisotropic material. As shown in Figure 1, three material directions can be distinguished in order to reduce the complexity of the material model: longitudinal (L), radial (R) and tangential (T). The developed material model is thus orthotropic with nine elastic constants. However, the same elastic properties were used for the radial and the tangential direction resulting in a smeared direction perpendicular-to-grain, i.e. $E_{22} = E_{33}$ and $G_{12} = G_{13}$. The logical choice of a transverse isotropic model cannot be used as five elastic constants are not enough to describe wood (would lead to a highly wrong rolling shear modulus G_{23}). The longitudinal direction corresponds to the direction parallel-to-grain. This is a similar build-up to fibre composites with a matrix (= 'perpendicular-to-grain') and main fibre direction (= 'parallel-to-grain') where e.g. fibre rupture in tension is a brittle failure mode and matrix failure in compression is ductile. These analogies motivated among others the choice of the CDM framework for wood material modelling as CDM methods are widespread approaches in composites modelling (e.g. Maimí [2006], Matzenmiller [1995]).

3   Continuum damage mechanics (CDM)

CDM is a nonlinear elastic approach where the nonlinear behaviour is obtained by modifying the stiffness matrix **D** or its inverse, the compliance matrix **C**. CDM can be implemented in an incremental-iterative FE framework. The stress increments are calculated from strain increments via a variable stiffness matrix. Therefore and as opposed to classical plasticity, the unloading in damage mechanics is following the secant stiffness and not following the elastic stiffness, see Figure 2. This approach can hence not model permanent plastic deformations.
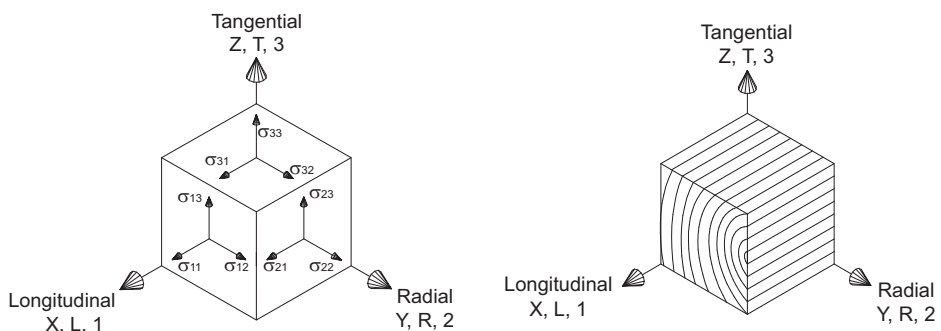

Figure 1. Definition of stress components and material directions

The basic principle of CDM is visualised in Figure 2. A damage variable d, $0 \leq d < 1$, is determined and inserted into the fundamental Hooke equation for linear elastic material as follows:

$$\sigma_{ij} = (1-d)D_{ijkl}\varepsilon_{kl} \tag{2}$$

If $d = 0$, no damage is present; if $d = 1$, the material has failed. In Equation (1), the scalar d describes isotropic damage. If anisotropic damage is observed, several damage variables **d** must be defined. Therefore, in order to develop a 3D material model for wood, three major mathematical definitions need to be established:

- Failure surfaces to identify damage initiation;
- Post-elastic behaviour when $0 < d < 1$;
- A constitutive model linking the stresses to the strains.

4   Damage initiation

Classical theory of plasticity is generally based on single-surface failure criteria that are not able to identify single failure modes. An example used in timber research is the already mentioned Tsai-Wu criterion [Tsai and Wu, 1971]. Therefore, in order to recognise failure modes, the single-surface has been subdivided; different failure criteria or damage initiation functions have been assigned to single stress components. This method is a well-known approach used in fibre composites (e.g. Maimí [2006], Matzenmiller et al. [1995], Hashin [1980]). For a complete 3D description of wood as an orthotropic material, eight stress-based failure criteria or damage initiation functions have been defined with f_x being
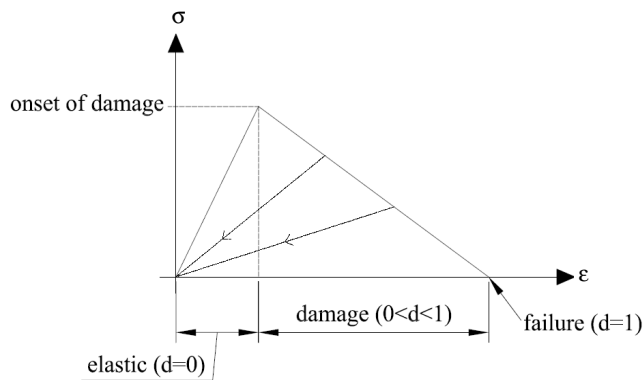

Figure 2. Basic idea of Continuum Damage Mechanics (CDM)

material strengths in tension (index t), compression (index c) and shear (indices v and $roll$) in parallel (index 0) and perpendicular (index 90) directions:

- $\sigma_L \geq 0$ - Criterion I: Failure in tension parallel-to-grain is a brittle failure mode of wood which is caused by tensile stresses σ_L parallel-to-grain. It is assumed that other stress components do not influence the tension strength parallel-to-grain. Maximum stress criterion:

$$F_{t,0}(\sigma) = \frac{\sigma_L}{f_{t,0}} \leq 1 \tag{3}$$

- $\sigma_L < 0$ - Criterion II: Failure in compression parallel-to-grain is a ductile failure mode of wood which is caused by compression stresses σ_L parallel-to-grain without interaction with other stress components. Maximum stress criterion:

$$F_{c,0}(\sigma) = \left| \frac{-\sigma_L}{f_{c,0}} \right| \leq 1 \tag{4}$$

The transverse tension modes and shear modes have to be combined as for instance splitting parallel to the LR-plane can be caused by tension perpendicular-to-grain (mode I), shear (mode II) or a combination of both (mixed mode). It is not possible to define separate failure modes for each stress component as degradation of one component also leads to degradation of the other components. This means that damage due to longitudinal shear also leads to damage in tension perpendicular-to-grain even though the actual tension stress component perpendicular-to-grain may still be lower than the tension strength perpendicular-to-grain.

- $\sigma_{R/T} \geq 0$ - Criteria III / IV: Failure in tension perpendicular-to-grain with splitting in LT-plane resp. in LR-plane is a brittle failure mode of wood which is caused by tensile stresses $\sigma_{R/T}$ perpendicular-to-grain, longitudinal shear stresses $\sigma_{LR/LT}$ and/or rolling shear stresses σ_{RT}. Quadratic criterion:

$$F_{t,90R/T}(\sigma) = \frac{\sigma_{R/T}^2}{f_{t,90}^2} + \frac{\sigma_{LT/LR}^2}{f_v^2} + \frac{\sigma_{RT}^2}{f_{roll}^2} \leq 1 \tag{5}$$

- $\sigma_{R/T} < 0$ - Criteria V-VIII: Two failure modes "pure transverse compression" and "shear", both occurring under compression perpendicular-to-grain, are distinguished. Failure in compression perpendicular-to-grain is a ductile failure mode of wood which is caused only by compression stresses $\sigma_{R/T}$ perpendicular-to-

grain. However, brittle shear failure can also occur if for instance the compression load is applied with an angle to the grain creating thus high shear stress components. Therefore, a failure criterion for shear stresses under simultaneous compression perpendicular-to-grain must be defined as well:

$$F_{c,90R/T}(\sigma) = \left| \frac{-\sigma_{R/T}}{f_{c,90}} \right| \leq 1 \tag{6}$$

$$F_{vR/T}(\sigma) = \frac{\sigma_{LT/LR}^2}{f_v^2} + \frac{\sigma_{RT}^2}{f_{roll}^2} \leq 1 \tag{7}$$

5   Damage evolution

After having identified damage initiation by means of Equations (3) to (7), the post-elastic mechanical behaviour and necessary damage variables need to be defined. After an extensive literature study on available experimental results [Sandhaas, 2012], two main post-elastic behaviour types were identified:

• ductile behaviour in compression parallel and perpendicular to the grain, Figure 3a.;
• softening behaviour in tension and shear where the shear is independent of the sign, Figure 3b.

As can be seen in Figure 3, simplified post-elastic laws were chosen as experimental evidence gives scattered and ambiguous results [Sandhaas, 2012]. Furthermore, in the author's opinion these two simplified laws are sufficient to model the main features of the mechanical behaviour of timber joints.
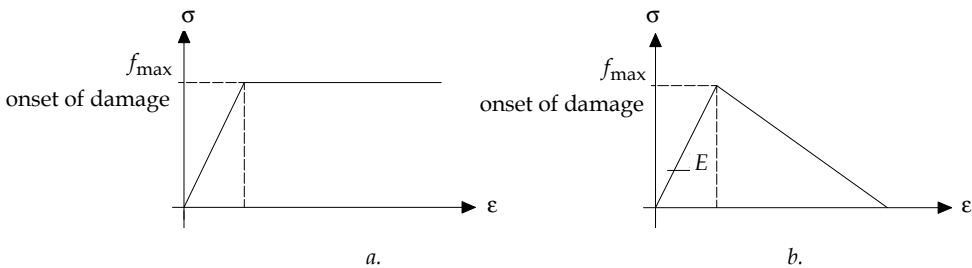

Figure 3. Stress-strain relationship; a. Elastic perfectly plastic behaviour, b. Softening behaviour

184

Exceeding the compression strength ($f_{c,0}$ and $f_{c,90}$) triggers ductile stress-strain behaviour where the damage variable follows an elastic perfectly plastic law, Figure 3a.:

$$\mathbf{d}(\boldsymbol{\kappa}) = 1 - \frac{1}{\boldsymbol{\kappa}} \tag{8}$$

The failure criteria for tension and shear instead lead to a linear softening stress-strain relationship as illustrated in Figure 3b.:

$$\mathbf{d}(\boldsymbol{\kappa}) = 1 - \frac{1}{f_{\max}^2 - 2G_f E}\left(f_{\max}^2 - \frac{2G_f E}{\boldsymbol{\kappa}} \right) \tag{9}$$

where $f_{\max}$ = maximum strength, E = modulus of elasticity, G_f = fracture energy.

As can be seen in Equations (8) and (9), the development of the damage variables is not depending on the strains $\boldsymbol{\varepsilon}$, but on state variables $\boldsymbol{\kappa}$ instead that keep track of the loading history [Maimí, 2006]. The damage variables cannot be a function of the strains $\boldsymbol{\varepsilon}$. For instance, once criterion III (= $F_{t,90R}$, splitting parallel to LT-plane) is activated due to high longitudinal shear stresses, the stiffnesses of all other contributing stress components (E_{22} and E_{23}) must degrade as well although the resp. uniaxial stresses σ_{22} and σ_{23} may still be below the uniaxial strengths $f_{t,90}$ and f_{roll} . In such a case, a dependency of the damage parameters $d_{t,90R}$ and d_{roll} on the strains ε_{22} and ε_{23} may not trigger the evolution of damage in these secondary directions.

The failure criteria $\mathbf{F}$ (Equations (3) to (7)) can be reformulated introducing these history parameters $\boldsymbol{\kappa}$:

$$\Theta(\mathbf{F}, \boldsymbol{\kappa}) = \mathbf{F} - \boldsymbol{\kappa} \leq 0 \tag{10}$$

This principle is analogous to the flow theory of plasticity. The "yield" surfaces $\mathbf{F}$ are the damage initiation functions or failure criteria. As in classical plasticity and following Maimí [2006], the Kuhn-Tucker conditions must hold:

$$\Theta \leq 0 \qquad \dot{\boldsymbol{\kappa}} \geq 0 \qquad \dot{\boldsymbol{\kappa}}\Theta = 0 \tag{11}$$

Furthermore, it is required that the damage variables can only grow which follows also from the second Kuhn-Tucker condition.

$$\dot{\mathbf{d}} \geq 0 \tag{12}$$

The final implementation of the history parameters as state variables is carried out as shown in Equation (13) where the superscript *incr* means that this update must be done at every increment up to the last increment *t*:

$$\kappa^t = \max\left\{1, \max_{incr=0,t}\left\{\mathbf{F}^{incr}\right\}\right\} \tag{13}$$

As the next step, the number of damage variables that control the post-elastic behaviour is established to nine:

- $d_{t,0}$ = damage in tension parallel-to-grain;
- $d_{c,0}$ = damage in compression parallel-to-grain;
- $d_{t,90R}$ = damage in tension perpendicular-to-grain, radial direction (*LT*-plane);
- $d_{c,90R}$ = damage in compression perpendicular-to-grain, radial direction;
- $d_{t,90T}$ = damage in tension perpendicular-to-grain, tangential direction (*LR*-plane);
- $d_{c,90T}$ = damage in compression perpendicular-to-grain, tangential direction;
- d_{vR} = damage in longitudinal shear, *LT*-plane;
- d_{vT} = damage in longitudinal shear, *LR*-plane;
- d_{roll} = damage in rolling shear, *RT*-plane.

A transgression of the damage initiation functions I to VIII (Equations (3) to (7)) activates the conjugated damage variables **d** where the shear damage variables can develop under transverse tension and transverse compression and have to be superposed.

The Macaulay operator as defined in Equation (14) is used to differentiate between damage variables that are activated by the same stress component, but are sensitive to the sign of the stress component, i.e. tension or compression stresses. Equation (15) shows an example how damage variables $d_{t,0}$ and $d_{c,0}$ can thus be expressed as damage variable d_0 .

$$\langle a \rangle := \frac{(a + |a|)}{2} \tag{14}$$

$$d_0 = d_{t,0}\frac{\langle \sigma_L \rangle}{|\sigma_L|} + d_{c,0}\frac{\langle -\sigma_L \rangle}{|\sigma_L|} \tag{15}$$

6 Constitutive model

CDM describes nonlinear material behaviour, especially softening behaviour, as caused by voids, defects or microcracks which reduce the area or volume of the material that can

transmit forces. The effective stress $\boldsymbol{\sigma}^{ef}$ is the stress acting on the non-damaged material. A simple relationship between effective stresses $\boldsymbol{\sigma}^{ef}$ and nominal stresses $\boldsymbol{\sigma}$ via the so-called damage operator $\mathbf{M}$ is shown in Equation (16). The damage operator $\mathbf{M}$ is composed by the nine damage variables $\mathbf{d}$ where the stress sign-dependent damage variables are combined as shown in Equation (15) for the damage variable parallel-to-grain d_0 .

$$\boldsymbol{\sigma}^{ef} = \mathbf{M}\boldsymbol{\sigma}$$

$$\mathbf{d} = \begin{bmatrix} d_0 & d_{90R} & d_{90T} & d_{vR} & d_{vT} & d_{roll} \end{bmatrix}^T$$

$$M_{ij} = \begin{cases} \begin{bmatrix} \dfrac{1}{1-d_0} & \dfrac{1}{1-d_{90R}} & \dfrac{1}{1-d_{90T}} & \dfrac{1}{1-d_{vR}} & \dfrac{1}{1-d_{vT}} & \dfrac{1}{1-d_{roll}} \end{bmatrix} & if \quad i = j \\[2mm] 0 & if \quad i \neq j \end{cases}$$

(16)

As the effective stress $\boldsymbol{\sigma}^{ef}$ is the stress acting on the (remaining) undamaged material, the constitutive relationship can also be formulated as shown in Equation (17) for a Hookean material with $\mathbf{D}^{el}$ the elastic stiffness matrix. Or, in the inverse formulation with the elastic compliance matrix $\mathbf{C}^{el}$:

$$\boldsymbol{\sigma}^{ef} = \mathbf{D}^{el}\boldsymbol{\varepsilon} \quad or \quad \boldsymbol{\varepsilon} = \mathbf{C}^{el}\boldsymbol{\sigma}^{ef}$$

(17)

Applying Equation (16), Equation (17) can then be reformulated for a damaged elastic compliance matrix $\mathbf{C}^{dam}$ (see also Matzenmiller et al. [1995]):

$$\boldsymbol{\varepsilon} = \mathbf{C}^{el}\boldsymbol{\sigma}^{ef} = \mathbf{C}^{el}\mathbf{M}\boldsymbol{\sigma} = \mathbf{C}^{dam}\boldsymbol{\sigma}$$

(18)

with $\mathbf{C}^{dam}$ according to Equation (19):

$$\mathbf{C}^{dam} = \mathbf{C}^{el}\mathbf{M} = \begin{bmatrix} \dfrac{1}{(1-d_0)E_{11}} & -\dfrac{v_{21}}{E_{22}} & -\dfrac{v_{31}}{E_{33}} & 0 & 0 & 0 \\[3mm] -\dfrac{v_{12}}{E_{11}} & \dfrac{1}{(1-d_{90R})E_{22}} & -\dfrac{v_{32}}{E_{33}} & 0 & 0 & 0 \\[3mm] -\dfrac{v_{13}}{E_{11}} & -\dfrac{v_{23}}{E_{22}} & \dfrac{1}{(1-d_{90T})E_{33}} & 0 & 0 & 0 \\[3mm] 0 & 0 & 0 & \dfrac{1}{(1-d_{vR})G_{12}} & 0 & 0 \\[3mm] 0 & 0 & 0 & 0 & \dfrac{1}{(1-d_{vT})G_{13}} & 0 \\[3mm] 0 & 0 & 0 & 0 & 0 & \dfrac{1}{(1-d_{roll})G_{23}} \end{bmatrix}$$

(19)

In finite element programmes, the inverse of the compliance matrix, the stiffness matrix $\mathbf{D}$ is needed in order to update the stresses:

$$\mathbf{D}^{dam} = \left(\mathbf{C}^{dam}\right)^{-1} \quad \Rightarrow \quad \boldsymbol{\sigma} = \mathbf{D}^{dam}\boldsymbol{\varepsilon} \tag{20}$$

If the compliance matrix is positive definite and $\mathbf{d} < 1$, this inverse exists.

In the damaged compliance matrix, damage effects and interactions have to be represented. For instance, damage in compression parallel-to-grain could be assumed to lead to a decrease of the stiffness in tension parallel-to-grain during a subsequent loading cycle. Furthermore, assumptions need to be made on the effects of damage parallel-to-grain on the strength perpendicular-to-grain.

In the developed material model, no damage interactions were modelled. For instance, it is assumed that damage in tension perpendicular-to-grain does not lead to a degradation of the properties parallel-to-grain.

Furthermore, when calculating the inverse of the damaged compliance matrix as given in Equation (19), non-diagonal, non-zero entries of the form $\nu_{ij}(\mathbf{d})$ containing Poisson's ratios and damage variables will be obtained in the damaged stiffness matrix. By means of the Poisson's ratios, the relationship between the normal stresses resp. strains is defined. Subsequently, these non-diagonal entries must also be adjusted taking damage into account: $\nu_{ij} = \nu_{ij}(\mathbf{d})$ [Matzenmiller et al., 1995].

It is safe to assume that with increasing damage also the Poisson's ratios will degrade. However, except for Franke [2008], no literature is known to the author where the evolution of the Poisson's ratios during a test was measured. Linear degradation as shown in Figure 4 or exponential degradation could be implemented. Here, the chosen Poisson's ratios have the value of the damaged Poisson's ratios already at the beginning of the modelling, see Figure 4. Therefore, the normal damage variables d_0 and $d_{90R/T}$ are considered to be decoupled.
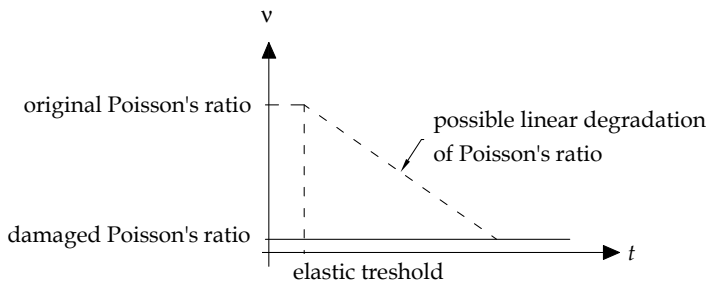

Figure 4.   Degradation of Poisson's ratios

7　Mesh regularisation

Every continuum mechanics approach with softening could suffer from mesh dependency problems. The source of mesh dependency is of mathematical nature as with the onset of softening, the previously well-posed problem has turned into an ill-posed problem. In computations, this results in a stiffness matrix which is no longer positive definite. The mathematical solution is a localisation zone of zero width without energy dissipation. The numerical solution tries to capture this physically inadmissible mathematical solution which yields a localised zone of smallest possible width, i.e. a single element in most cases. In literature, many different regularisation methods are available (e.g. Sluys [1992]). Here, the crack band method as described in Bažant and Oh [1983] was chosen to regularise the mesh. With the crack band method, the fracture energy is expressed in terms of characteristic finite element length h, where h is a geometrical value in [length] containing information on the element's aspect ratio:

$$g_f = \frac{G_f}{h} \tag{21}$$

In Equation (21), the fracture energy G_f needs to be replaced by the characteristic fracture energy g_f if the crack band model is activated. The introduction of a characteristic fracture energy g_f that is correlated to the element size provides the transformation of the fracture energy G_f into a 'mesh-dependent' value. For instance, in a coarse mesh, h will be large and leads hence to a small characteristic fracture energy g_f in comparison to the large g_f of a fine mesh with a small characteristic element length h. This adjustment of the fracture energy considering the mesh size compensates for the trend of continuum softening models to dissipate as little energy as possible. However, the crack band model only works if one failure mode is dominating and if a localised solution occurs. It is valid if damage develops only in a band of elements and not in all elements homogeneously.

8　Viscous stabilisation

Viscous stabilisation similarly to Maimí [2006] is used in order to improve the convergence characteristics of the developed material model. A fictitious viscous parameter η is introduced in the model. Due to the additional viscous component, the stiffness matrix is generally positive definite. Therefore, viscous stabilisation leads to a more robust solution process with less convergence problems.

As viscosity is a time-dependent material parameter, viscous stabilisation must be a function of the rate of damage. The rate of the damage variable or of the damage threshold (= failure criteria) may be used. Equation (22) shows the stabilisation as a function of rate of damage variables:

$$\dot{d} = \frac{(d - d_V)}{\eta} \tag{22}$$

In Equation (22), the viscous parameter η defines the rate at which the true damage d and the stabilised damage d_V as defined in Equation (23) approach each other. Equation (22) can now be discretised in time. Equation (23) shows the discretised equation based on the backward Euler algorithm to insert an artificial viscosity η that is acting on the damage variables.

$$d_V^t = \max\left\{0, d_V^{t-1}, \frac{\eta}{\eta + dt} d_V^{t-1} + \frac{dt}{\eta + dt} d^t\right\} \tag{23}$$

As viscous stabilisation is applied to improve convergence, the energy output must be controlled in order to judge the model performance and reliability, i.e. to control that fictitious viscosity is not influencing modelling results. To this scope, the total dissipated energy and the dissipated energy associated with viscous regularisation are calculated as internal state variables. Both variables do not have any influence on the solution. They are merely used for energy output, control and post processing.

9   Material properties

A major issue of all material models is the need of mechanical input parameters such as stiffness and strength values which usually derive from tests. The developed wood model needs seventeen properties as listed in .

Table 1 for three different wood species.
Generally, stiffness and strength values can be procured only with difficulty. This is due to two main issues. Firstly, the inherent large scatter of mechanical properties for wood and secondly, difficulties connected with testing and measuring. For instance, the uniaxial shear strength can hardly be assessed without triggering stress peaks or secondary stresses [Moses and Prion, 2004]. Furthermore, not always all parameters are measured, e.g. due to Poisson effect, or the positioning of the measuring instruments is not clear.

As for stiffness values given in material standards such as EN 338 for instance, they usually derive from large-scale four-point bending tests and not necessarily provide significant values for material models.

Also the fracture energies suffer from a large scatter and the fact that they are usually measured on small clear wood specimens whereas for a heterogeneous material, it can be safely assumed that fracture energies are not constant. Moreover, the needed material values are rather easily procurable for softwoods, but not for hardwoods.

In Sandhaas [2012], a thorough literature study has been carried out where the issues around reliable material parameters are discussed and the chosen values from Table 1 are motivated.

Table 1.   Material properties for spruce, beech and azobé (variation A beech needed later)

Parameters	Units	Spruce (*Picea abies*)	Beech (*Fagus silvatica*)	Azobé (*Lophira alata*)	Variation A Beech
E_{11}	MPa	11000	13000	20000	13000
$E_{22} = E_{33}$	MPa	370	860	1330	860
$G_{12} = G_{13}$	MPa	690	810	1250	810
G_{23}	MPa	50	59	91	59
$f_{t,0}$	MPa	24	41	72	41
$f_{c,0}$	MPa	36	45	58	45
$f_{t,90}$	MPa	0.7	1.0	1.0	**10**
$f_{c,90}$	MPa	4.3	14.2	23.2	14.2
f_v	MPa	6.9	6.9	8.6	**10**
f_{roll}	MPa	0.5	0.5	0.6	**10**
$G_{f,0}$	N/mm	60	100	180	100
$G_{f,90}$	N/mm	0.5	0.71	0.71	**50**
$G_{f,v}$	N/mm	1.2	1.2	1.5	**50**
$G_{f,roll}$	N/mm	0.6	0.6	0.7	**10**
η	-	0.0001	0.0001	0.0001	0.0001

10 Modelling

The developed material model was programmed in a user subroutine `UMAT` and inserted into the commercial FE software ABAQUS. The subroutine is given in Sandhaas [2011]. All validations that are necessary when developing a constitutive model can be found in Sandhaas [2012]. Different models were run ranging from modelling compression or tension tests on wood over embedment models to joint models. In this paper, some embedment models are chosen in order to show the capabilities of the developed constitutive model.

Embedment models were thus developed whose outcomes could be verified with tests taken from literature [Sandhaas et al., 2010]. Three different wood species were chosen, spruce, beech and azobé. The material properties are given in .

Table 1. The FE model is shown in Figure 5, only a quarter of an embedment specimen with a 24 mm dowel was modelled. As no localised damage is expected, the crack band model was deactivated. 3D solids with linear interpolation between the eight integration points were chosen. Friction between dowel and wood was simulated with the stick-slip model and a friction coefficient of μ = 0.5. This is a simplified assumption for contact modelling, other novel approaches can e.g. be found in Dorn [2012].
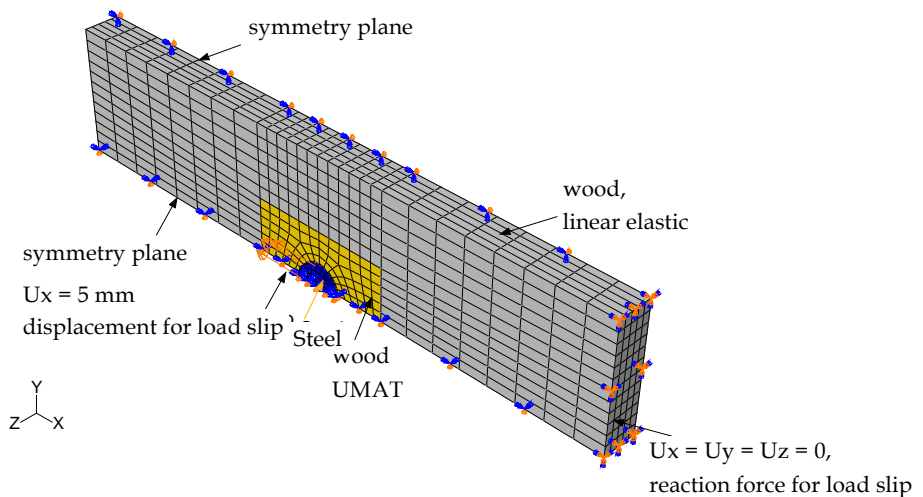

Figure 5. Quarter of embedment model with boundary conditions, materials and default mesh

As an example, Figure 6 shows the modelling outcomes of an embedment model in comparison with a typical embedment test result on spruce. In Figure 6a., damage due to compression parallel-to-grain directly underneath the dowel of a spruce specimen can be clearly seen. Also brittle damage due to tension perpendicular-to-grain is identified, Figure 6c. The damage variable $d_{t,90}$ in Figure 6c. shows the damage development due to shear as both failure modes are coupled as defined in Equation (5).

In Figure 6c, two elements are indicated whose integration point results in terms of tension perpendicular-to-grain and longitudinal shear are given in Figure 7. It can be seen that damage in element a initiated due to high shear stresses σ_{12} (f_v = 6.9 MPa, Figure 7a.) and in element b, damage was triggered by high tension stresses perpendicular-to-grain σ_{22} ($f_{t,90}$ = 0.7 MPa, Figure 7b.). Both predictions are correct if the position of the elements in the model is considered.

Figure 9 shows load-slip graphs of azobé specimens in overlap with the modelling result. The stiffness prediction is good. The reached displacement was too low. However, the source of the brittle failure observed in Figure 9 at a displacement of less than 1 mm is purely numerical and is not expressing the global splitting of the embedment model. The load drop of the simulated load-slip graph represents a numerical failure with no physical meaning other than that the wood underneath the dowel is collapsed completely being thus an artificial softening. Once the row of elements directly underneath the dowel fails, spurious energy modes develop in the used elements. The load cannot be transferred to neighbouring elements as they are already unloading although they may not have reached

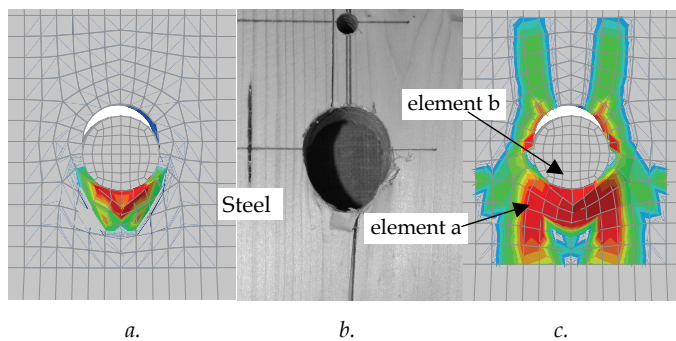a.   b.   c.

Figure 6. Embedment of spruce with 24 mm dowel; a. Damage variable $d_{c,0}$ in compression parallel-to-grain, b. Test result, c. Variable $d_{t,90}$ in tension perpendicular-to-grain (A colour figure is available at www.heronjournal.nl)
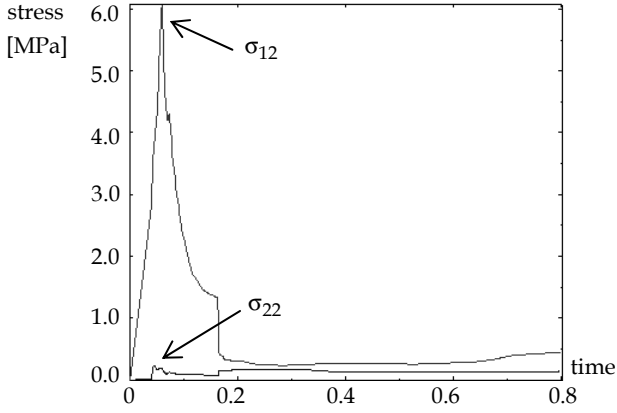
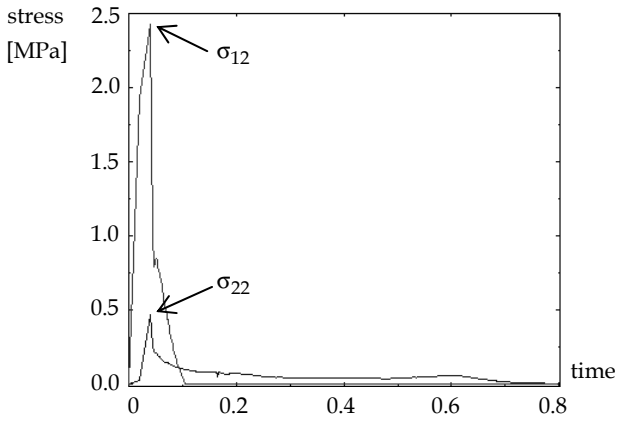*Figure 7a. Stress components σ$_{22}$ and σ$_{12}$ of element a*

Figure 8b. Stress components σ$_{22}$ and σ$_{12}$ of element b (Figure 6)
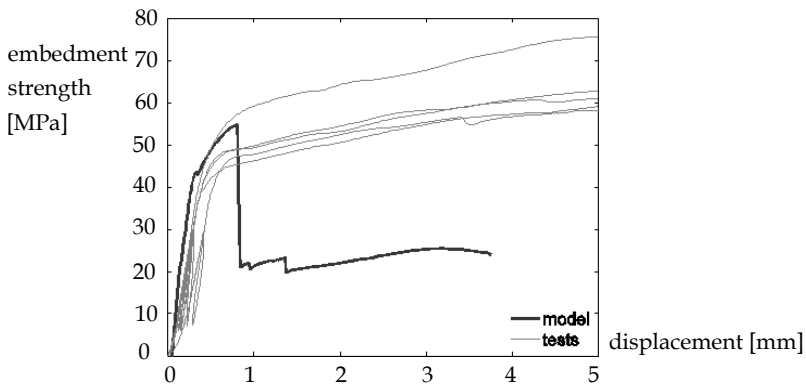

Figure 9. FE result versus test results of embedment tests on azobé with 24 mm dowels

194

their ultimate load carrying capacity yet. Basically, the model fails completely on a local level of collapsed elements whereas the neighbouring elements still can carry load.

Accordingly, there are three main options to improve the model performance and to avoid local early brittle failures due to spurious energy modes:

- Introduction of a threshold value for the damage variables in order to avoid complete damage and to keep a residual stiffness. This however is not thought to be a good solution as an uncontrollable fictitious parameter would be introduced.
- Change resp. increase mechanical properties in order to avoid early complete damage of elements. Again, this is not thought to be a good solution as the material properties should be comprehensible and not arbitrarily changed with the scope to make a model work.
- Use different element formulations or e.g. arbitrary Lagrangian-Eulerian (ALE) approaches (e.g. Rodríguez-Ferran et al. [2002]) to control excessive mesh distortion.

Point three is part of future research as then, the material subroutine will be optimised and solutions will be developed to control excessive element distortion.
The second option however was carried out in order to understand the influence of the material parameters. Also considering the rather difficult determination of certain material properties such as the fracture energies or the fact that the chosen strength values (especially perpendicular-to-grain and shear values) as given in .

Table 1 are based on mean values for structural wood and are thus low in comparison with defect-free wood, it is thought to be admissible to modify these parameters. Around the dowel, usually no knots are present and the local material properties can safely be assumed to be higher than the properties for structural wood. .

Table 1 gives modified material parameters for beech wood nominated "variation A" where the properties controlling the 3D brittle behaviour are increased. Figure 10 shows the modelling results for an embedment test specimen with the default properties for beech and variation A superposed with test results. The load-slip behaviour applying the default properties shows again too brittle behaviour due to numerical softening. However, "variation A" reaches higher deformations before failure. The higher values for strength and fracture energies as defined for "variation A" lead to numerical softening at higher deformations which is more realistic.

195

As the resulting curve for "variation A" still yields too high strength values, also the compression strength parallel-to-grain is reduced as indicated in Figure 10. Such a reduction is thought to reduce the load carrying capacity and should therefore lead to a lower plateau.

Modelling outcomes confirmed this. A better agreement between tests and model can thus be obtained by modifying certain mechanical properties. However, this is arbitrary and highlights the difficulties associated with a correct identification of material input parameters.

Another important outcome of modelling can also be deduced from Figure 10. The earlier initiation of damage in the default model with a decrease in stiffness in comparison to "variation A" is clearly observable in the detail (lower stiffness of the red line of default model in comparison to the blue line of "variation A"). The global stiffness is thus decreasing due to damage in tension perpendicular-to-grain and shear (properties that have been changed according to .

Table 1) although the model still shows a very clear load increase. This is a realistic prediction.

11   Conclusions

A promising constitutive 3D model for the material wood was developed that can identify failure modes and combine simultaneous ductile and brittle failures within one model. The mechanical material parameters needed for the constitutive relationship are clearly defined. The material model runs in a complex FE environment in combination with other material models and contact formulations.

Modelling results were satisfying in terms of stiffness and load carrying capacity. Artificial softening caused by spurious energy modes of completely collapsed elements however led to early brittle failure of models that did not represent physical failure. Furthermore, once unloading has started in the most stressed elements, the load is not transferred to neighbouring elements. These numerical problems need to be solved in order to optimise the subroutine.

As for any other modelling approach, a major issue lies in the determination of the necessary mechanical properties. As the model performance and prediction capacity is highly dependent on these properties, methods to derive reliable values must be developed.
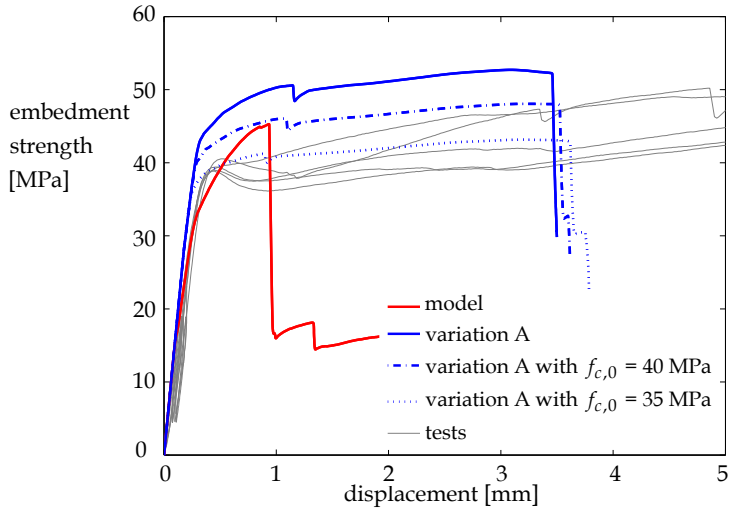
Figure 10. FE result versus test results of embedment tests on beech with 24 mm dowels, material parameters modified – variation A

Literature

Ballerini, M. and Rizzi, M. (2005). A numerical investigation on the splitting strength of beams loaded perpendicular-to-grain by multiple dowel-type connections. *CIB-W18 Meeting 38*. Karlsruhe, Germany, Paper 38-7-1.

Bažant, Z.P. and Oh, B.H. (1983). Crack band theory for fracture of concrete. *Matériaux et Constructions*, 16:155-177.

Bocquet, J.F. (1997). *Modélisation des déformations locales du bois dans les assemblages brochés et boulonnés*. PhD thesis, Université Blaise Pascal Clermont-Ferrand.

Bouchaïr, A. and Vergne, A. (1995). An application of the Tsai criterion as a plastic-flow law for timber bolted joint modeling. *Wood Science and Technology*, 30:3-19.

Dias, A.M.P.G., Van de Kuilen, J.W.G., Cruz, H.M.P. and Lopes, S.M.R. (2010). Numerical modelling of the load-deformation behavior of doweled softwood and hardwood joints. *Wood and Fiber Science*, 42:480-489.

Dorn, M. (2012). *Investigations on the serviceability limit state of dowel-type timber connections*. PhD thesis, Technische Universität Wien.

Fleischmann, M. (2005). *Numerische Berechnung von Holzkonstruktionen unter Verwendung eines realitätsnahen orthotropen elasto-plastischen Werkstoffmodells*. PhD thesis, Technische Universität Wien.

Franke, S. (2008). *Zur Beschreibung des Tragverhaltens von Holz unter Verwendung eines photogrammetrischen Messsystems*. PhD thesis, Bauhaus-Universität Weimar.

Grosse, M. (2005). *Zur numerischen Simulation des physikalisch nichtlinearen Kurzzeit-tragverhaltens von Nadelholz am Beispiel von Holz-Beton-Verbundkonstruktionen*. PhD thesis, Bauhaus-Universität Weimar.

Hashin, Z. (1980). Failure criteria for unidirectional fiber composites. *Journal of Applied Mechanics*, 47:329-33.

Hofstetter, K., Hellmich, C. and Eberhardsteiner, J. (2005). Development and experimental validation of a continuum micromechanics model for the elasticity of wood. *European Journal of Mechanics A/Solids*, 24:1030-1053.

Maimí, P. (2006). *Modelización constitutiva y computa-cional del daño y la fractura de materiales compuestos*. PhD thesis, Universitat de Girona.

Matzenmiller, A., Lubliner, J. and Taylor, R.L. (1995). A Constitutive Model for Anisotropic Dam-age in Fiber-Composites. *Mechanics of Materials*, 20:125-152.

Moses, D.M. and Prion, H.G.L. (2004). Stress and failure analysis of wood composites: a new model. *Composites Part B-Engineering*, 35:251-261.

Nagy, E. (2010). *A lattice model for the prediction of the mechanical properties of certain softwoods*. PhD thesis, University of Maine.

Reichert, T. (2009). *Development of 3D lattice models for predicting nonlinear timber joint behaviour*. PhD thesis, Napier University Edinburgh.

Rodríguez-Ferran, A., Pérez-Foguet, A. and Huerta, A. (2002). Arbitrary Lagrangian-Eulerian (ALE) formulation for hyperelastoplasticity. *International Journal for Numerical Methods in Engineering*, 53:1831-1851.

Sandhaas, C. (2012). *Mechanical behaviour of timber joints with slotted-in steel plates*. PhD thesis, University of Technology Delft.

Sandhaas, C. (2011). 3D Material Model for Wood, Based on Continuum Damage Mechanics. Stevinrapport 6-11-4, Stevin II Laboratory, *University of Technology Delft*.

Sandhaas, C., Van de Kuilen, J.W.G., Blass, H.J. and Ravenshorst, G. (2010). Embedment tests parallel-to-grain and ductility in tropical hardwood species. *Proceedings WCTE*. Riva del Garda, Italy.

Schmid, M. (2002). *Anwendung der Bruchmechanik auf Verbindungen mit Holz*. PhD thesis, Technische Universität Karlsruhe.

Schmidt, J. and Kaliske, M. (2006). Zur dreidimensionalen Materialmodellierung von Fichtenholz mittels eines Mehrflächen-Plastizitätsmodells. *Holz als Roh- und Werkstoff*, 64:393-402.

Sluys, L.J. (1992). *Wave Propagation, Localisation and Dispersion in Softening Solids*. PhD thesis, Technische Universiteit Delft.

Toussaint, P. (2010). *Application et modélisation du principe de la précontrainte sur des assemblages de structure bois*. PhD thesis, Université Henri Poincaré Nancy.

Tsai, S.W. and Wu, E.M. (1971). A general theory of strength for anisotropic materials. *Journal of Composite Materials*, 5:58-80.

Wittel, F.K., Dill-Langer, G. and Kröplin, B.H. (2005). Modeling of damage evolution in soft-wood perpendicular to grain by means of a discrete element approach. *Computational Materials Science*, 32:594-603.

Xu, B.H., Taazount, M., Bouchaïr, A. and Racher, P. (2009). Numerical 3D finite element modelling and experimental tests for dowel-type timber joints. *Construction and Building Materials*, 23:3043-3052.

European standards:

EN 338:2009. Structural Timber – Strength classes. CEN European Committee for Standardisation, Brussels, 2009.

Finite Element Software package:

ABAQUS Version 6.8, Dassault Systèmes Simulia Corp., Providence, RI, USA, 2008.